







## RESEARCH ARTICLE

**VRK1 (Y213H) homozygous mutant impairs Cajal bodies in a hereditary case of distal motor neuropathy**

Ana T. Marcos<sup>1,\*</sup> , Elena Martín-Doncel<sup>2,3,\*</sup> , Patricia Morejón-García<sup>2,3</sup> , Iñigo Marcos-Alcalde<sup>4,5</sup> , Paulino Gómez-Puertas<sup>4</sup> , María Segura-Puimedon<sup>6</sup> , Lluís Armengol<sup>6</sup> , José M. Navarro-Pando<sup>1,7,8</sup>  & Pedro A. Lazo<sup>2,3</sup> 

<sup>1</sup>Unidad de Genética, Instituto para el Estudio de la Biología de la Reproducción Humana (INEBIR), Sevilla, Spain

<sup>2</sup>Molecular Mechanisms of Cancer Program, Instituto de Biología Molecular y Celular del Cáncer, Consejo Superior de Investigaciones Científicas (CSIC), Universidad de Salamanca, Salamanca, Spain

<sup>3</sup>Instituto de Investigación Biomédica de Salamanca (IBSAL), Hospital Universitario de Salamanca, Salamanca, Spain

<sup>4</sup>Molecular Modelling Group, Centro de Biología Molecular "Severo Ochoa", CSIC-Universidad Autónoma de Madrid, Cantoblanco, Madrid, Spain

<sup>5</sup>School of Experimental Sciences, Biosciences Research Institute, Universidad Francisco de Vitoria, Pozuelo de Alarcón, Madrid, Spain

<sup>6</sup>Quantitative Genomic Medicine Laboratories, qGenomics, Espluges de Llobregat, Barcelona, Spain

<sup>7</sup>Cátedra de Reproducción y Genética Humana, Facultad de Ciencias de la Salud, Universidad Europea del Atlántico, Santander, Spain

<sup>8</sup>Fundación Universitaria Iberoamericana (FUNIBER), Barcelona, Spain

**Correspondence**

Pedro A. Lazo, Instituto de Biología Molecular y Celular del Cáncer, CSIC-Universidad de Salamanca, Campus Miguel de Unamuno s/n, 37007 Salamanca, Spain. Tel: +34 923 294 804; Fax: +34 923 194 795; E-mail: pedro.lazo@csic.es

**Funding Information**

E. M-D., and P. M-G. were supported by Junta de Castilla y León-Fondo Social Europeo (ESF), and Ministerio de Educación-FPU predoctoral (FPU16/01883) fellowships, respectively. This work was funded by grants from Ministerio de Ciencia, Innovación y Universidades-Agencia Estatal de Investigación (SAF2016-75744-R, RED2018-102801-T) and Consejería de Educación-Junta de Castilla y León-ERDF (UIC-258) to P.A.L. Ministerio de Ciencia, Innovación y Universidades-Agencia Estatal de Investigación (RTC-2017-6494-1 and RTI2018-094434-B-I00) and European Commission project "CONNECT-JPIAMR" Virtual Research Institute to P.G-P. The Instituto de Biología Molecular y Celular del Cáncer is cofunded by Junta de Castilla y León-European Regional Development Fund (CLC-2017-01).

Received: 8 February 2020; Revised: 27 March 2020; Accepted: 31 March 2020

doi: 10.1002/acn3.51050

**Abstract**

**Background:** Distal motor neuropathies with a genetic origin have a heterogeneous clinical presentation with overlapping features affecting distal nerves and including spinal muscular atrophies and amyotrophic lateral sclerosis. This indicates that their genetic background is heterogeneous. **Patient and methods:** In this work, we have identified and characterized the genetic and molecular base of a patient with a distal sensorimotor neuropathy of unknown origin. For this study, we performed whole-exome sequencing, molecular modelling, cloning and expression of mutant gene, and biochemical and cell biology analysis of the mutant protein. **Results:** A novel homozygous recessive mutation in the human *VRK1* gene, coding for a chromatin kinase, causing a substitution (c.637T > C; p.Tyr213His) in exon 8, was detected in a patient presenting since childhood a progressive distal sensorimotor neuropathy and spinal muscular atrophy syndrome, with normal intellectual development. Molecular modelling predicted this mutant *VRK1* has altered the kinase activation loop by disrupting its interaction with the C-terminal regulatory region. The p.Y213H mutant protein has a reduced kinase activity with different substrates, including histones H3 and H2AX, proteins involved in DNA damage responses, such as p53 and 53BP1, and coilin, the scaffold for Cajal bodies. The mutant *VRK1*(Y213H) protein is unable to rescue the formation of Cajal bodies assembled on coilin, in the absence of wild-type *VRK1*. **Conclusion:** The *VRK1*(Y213H) mutant protein alters the activation loop, impairs the kinase activity of *VRK1* causing a functional insufficiency that impairs the formation of Cajal bodies assembled on coilin, a protein that regulates *SMN1* and Cajal body formation.

\*Equal contributing first authors.

## Introduction

Hereditary neuropathies are characterized by involvement of motor, sensory, and/or autonomic nerve fibers,<sup>1</sup> and are divided into three main categories: hereditary motor and sensory neuropathies (HMSN), also known as Charcot–Marie–Tooth (CMT) disease, hereditary motor neuropathy, and hereditary sensory and autonomic neuropathy (HSAN).<sup>2</sup> Distal neuropathies and spinal muscular atrophy (SMA) are progressive diseases affecting the lower motor neurons and characterized for a progressive muscle loss and weakness, and have overlapping symptoms.<sup>3</sup> The most common forms of these diseases are associated with deletions or mutations in *CMT* genes, or in the exon of the *SMN1* gene that is not compensated by *SMN2*<sup>3,4</sup> and is involved in RNA processing mediated by snRNP.<sup>5</sup> However, there is heterogeneity in disease presentation, evolution and manifestations, which has led to the identification of novel genes implicated in the pathogenesis of these diseases.<sup>3</sup> These include alterations in mechanisms that regulate RNA splicing and processing, or in the subcellular structures where these functions take place, such as Cajal bodies.

Cajal bodies (CBs) are assembled on coilin.<sup>6,7</sup> CBs organization and assembly are lost by either *SMN1* depletion,<sup>8</sup> or *VRK1* depletion,<sup>7</sup> and both form part of a common complex.<sup>6,7</sup> Coilin also forms complexes with splicing snRNP.<sup>9–11</sup> Moreover, both *SMN1*<sup>12</sup> and *VRK1*<sup>13</sup> bind to chromatin. Coilin levels and its posttranslational modifications also affect RNA processing and splicing.<sup>14</sup> In this context, *VRK1* phosphorylates coilin in Ser184 and regulates its stability and assembly by protecting it from ubiquitin-mediated proteasomal degradation in the cytosol, facilitating its nuclear accumulation,<sup>7</sup> and also interacts with Heterogeneous nuclear ribonucleoprotein A1 (hnRNP A1) and regulates telomerase activity and telomere maintenance.<sup>15</sup> CBs alterations can be alternative pathogenic routes leading to distal neuromotor syndromes, and in which multiple genes have been implicated.<sup>16</sup>

Several very rare recessive mutations in the human *VRK1* gene, either homozygous or compound heterozygous, have been detected in diseases affecting the motor neuron, which have a phenotypic heterogeneity in their clinical presentation.<sup>17–24</sup> These *VRK1* mutations are recessive, and all of them are very rare, some hereditary, and others de novo. Among the distal motor neuropathy phenotypes associated with human *VRK1* mutations are SMA,<sup>17,20,23–25</sup> ALS,<sup>19,20</sup> and pontocerebellar hypoplasia.<sup>17</sup>

In this work, we have identified a novel homozygous recessive mutation in the human *VRK1* gene, and the mutant protein has altered the folding of its activation loop that prevents the activation of the kinase activity leading to a deficiency in the assembly of Cajal bodies.

## Patient, Materials, and Methods

### Clinical characteristics of the patient

The patient, son of consanguineous parents and currently 35 years, presented initial symptoms at 4 years with a progressive distal muscle weakness in legs and arms that became much more severe with time. The child has a foot deformity with pes cavus and bilateral foot drop, leading to unstable walk with distal amyotrophy of lower and upper members. Electromyogram, performed at 9 years, detected a significant slowdown of motor and sensory nerve conduction velocity. At 16 years required foot surgical correction to allow for adequate standing. The disease progressed with time needing walking stick, and currently is wheel chair bound. At 24 years there was a significant loss of muscle strength, unable to raise from sedation without help, and at 34 years the patient cannot use hands for feeding or writing. Normal intellectual development and normal speech.

The parents are consanguineous first cousins, and the father has epilepsy. Both parents have pes cavus.

### Whole-exome sequencing

For whole-exome sequencing (WES), DNA was extracted from peripheral blood of the patient using the Maxwell 16 system. DNA quality was determined measuring optical density with a DeNovix DS-11. Human exome was enriched using the MedExome SeqCap EZ assay (Roche-Nimblegen, CA), and sequenced using a NextSeq 500 (Illumina, CA) equipment. An average 71x coverage depth was achieved along the target regions (exons and  $\pm 75$  intronic nucleotides flanking the exon–intron boundaries). Variants were identified by alignment of reads against the Human reference genome sequence (hg19), using BWA-0.7–12, GATK-3.5 procedures for the detection of single nucleotide variants and indels and exome depth for deletions and duplications. Annotation of the variants was performed using Annovar (2016Feb01) and filtering and prioritization was performed using public (1000 genomes, Genome Aggregation Database and Exome Variant Server) databases in order to identify candidate variants related to the clinical

phenotype. Variants were classified following the American College of Medical Genetics and Genomics (ACMG) guidelines,<sup>26,27</sup> Polyphen-2<sup>28</sup> and VarElect<sup>29</sup> algorithms were used to predict the effect of the variants. Sanger sequencing in the index case, parents, and siblings was performed to confirm the variant and to determine its inheritance pattern.

### Ethical compliance

The genomic study was performed for diagnosis in a case of unknown origin and was approved by the Institutional review board. Informed consent was obtained from each subject.

### Molecular modeling of structure

The 3D structure of the human Vaccinia-Related Kinase 1 (VRK1) wild-type protein was obtained from the Protein Data Bank (PDB id: 2LAV).<sup>30</sup> The dynamic molecular modeling methods are described in Data S1.

### Cloning of altered VRK1 gene, plasmids, and mutagenesis

Human VRK1 was expressed from mammalian expression vector, pCEFL-HA-VRK1,<sup>31</sup> and bacterial expression pGEX-4T-VRK1.<sup>31–34</sup> The Y213H mutation was introduced in these plasmids with the GeneArt Site-Directed Mutagenesis System (Invitrogen-ThermoFisher). The primers for human VRK1-p.Y213H were: forward (5'-AGGAGTTCATAAAGAACACAAAGAAGACCCCAAAA-3'), and reverse (5'-TTTTGGGGTCTTCTTTGTGTCTTTATGAACTCCT-3'). VRK1 wild-type and the p.Y213H variant proteins were expressed in *E.coli* from constructs made in plasmid pGEX4T-GST-VRK1 for bacterial expression,<sup>32</sup> or in pCEFL-HA-VRK1 for expression in mammalian cells.<sup>34</sup> The human Y213H mutation was introduced in murine VRK1 (mVRK1) and cloned in pCEFL-Myc-mVRK1 to generate pCEFL-Myc-mVRK1 (Y213H) plasmid. The primers used for murine VRK1-Y213H forward (5'-TGGAGTTCATAAAGAGCACAAAGGAAGATCCCAAAA-3') and reverse (5'-TTTGGGA TCTTCCTTGACTCTTTATGAACTCCA-3). Full methods are in Data S1.

### Kinase assays

Kinase assays were performed as previously described.<sup>31,34,35</sup> Briefly, in vitro kinase assays with [<sup>32</sup>P]- $\gamma$ ATP were performed with GST-VRK1 wild-type, or the p.Y213H variant.<sup>7,31,36</sup> Kinase assays with the following substrates were previously published: histone H3,<sup>13,33</sup>

H2AX,<sup>13</sup> p53,<sup>37,38</sup> 53BP1,<sup>39</sup> and coilin.<sup>7</sup> Full methods are in Data S1.

### Cell lines, transfections, and protein analysis

All molecular and cellular methods have been reported before and are detailed in cellular and in Data S1.<sup>34</sup> Antibodies are in Table S1.

## Results

### Genetic findings

Whole-exome sequencing detected in the patient a homozygous mutation (NM\_003384:exon8:c.T637C:p.Y213H) in exon 8 of the VRK1 gene. This mutation was detected in heterozygosis in both consanguineous parents, and the two siblings of the patient (Fig. 1). Heterozygous carriers have no neurological pathology.

### Molecular modeling of VRK1(Y213H) variant protein and functional prediction

Polyphen-2 analysis of this aminoacid substitution predicts the highest damaging score. VarElect analysis predicts a very high likelihood of causing a neuropathy and muscular atrophy.<sup>29</sup> To study the effect of the VRK1(Y213H) mutant protein, the 3D structure of human VRK1 protein (2LAV) was obtained from the Protein Data Bank.<sup>30</sup> This structure includes the position of the protein C-terminal tail, as well as the structure of the VRK1 activation loop, where the Tyr213 residue is located (Fig. S1). Tyr213 forms a T-shaped stacking complex with Tyr311, located in an alpha helix close to the activation loop (Fig. S1). This type of Tyr-Tyr interactions has been shown as contributing to structural protein stability,<sup>40</sup> as is the case of the VRK1 activation loop. The mutant residue VRK1(Y213H) is located in the activation loop of the kinase.<sup>30</sup> To detect the structural consequences of the Y213H mutant, models for wild-type (VRK1-WT), and Y213H mutant (VRK1-Y213H) proteins were subjected to 200 nsec of free molecular dynamic (MD) simulation. The activation loop of the VRK1-WT structure did not experience noticeable variations during the molecular dynamics trajectory, remaining virtually unchanged after 200 nsec of MD (Fig. 2A). The only variation suffered by the activation loop was the stabilization of the C-terminal end of the protein, through the formation of saline bridges between the negative amino acid Glu361 and the positive residues Lys211 and Arg219 of the loop (Fig. 2A). This interaction remained stable for more than 40% of the total simulation time. After 200 ns of molecular dynamics (MD), the 3D structure of the

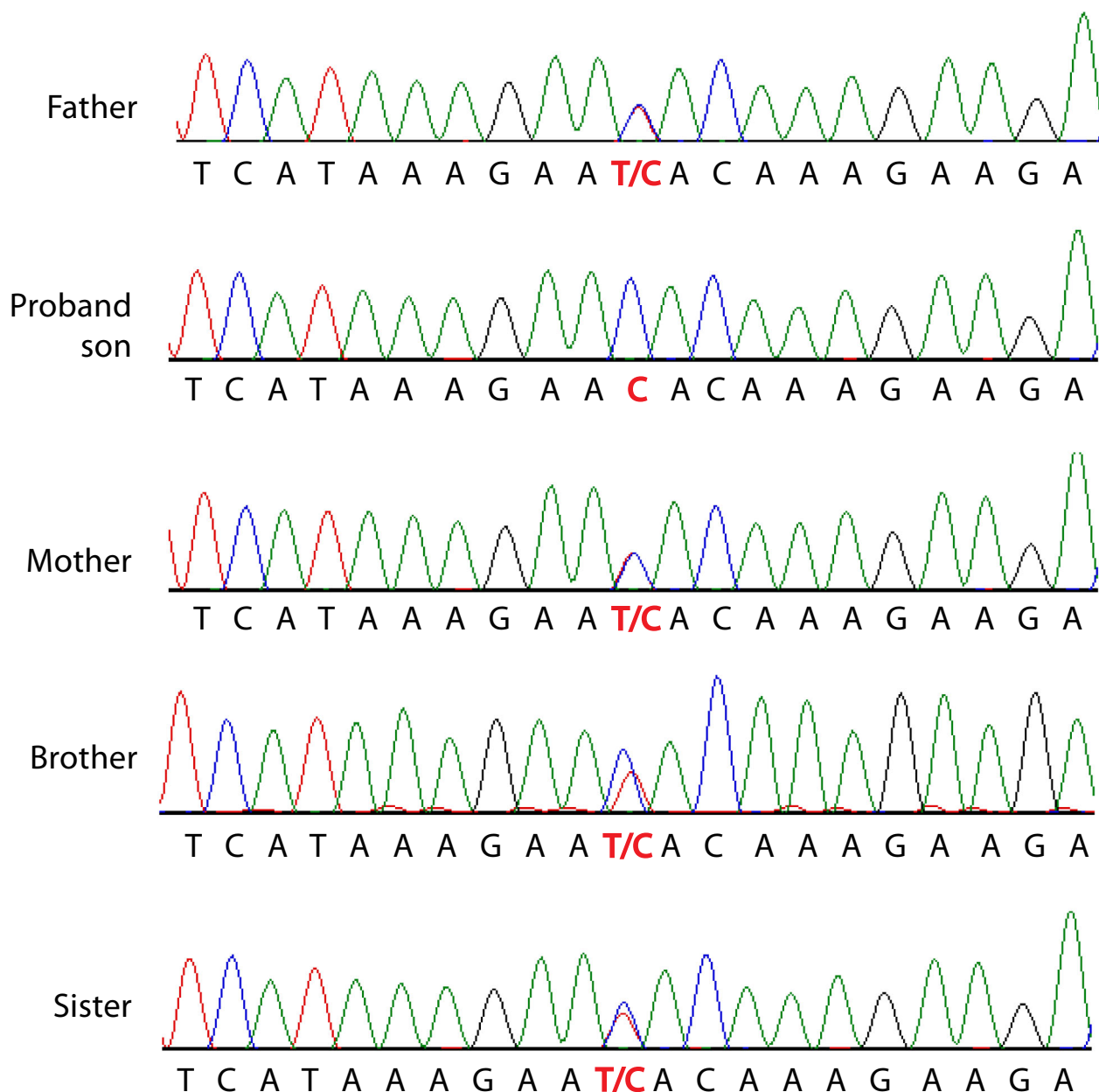


**Figure 1.** Identification of a novel mutation in the human *VRK1* gene coding for a nucleosomal kinase. Detection and confirmation of the *VRK1* mutation in the five members of the family.

VRK1(Y213H) mutant activation loop displayed a different arrangement (Fig. 2B). His213 continued to interact with Tyr311 but in the form of a parallel-displaced stacking, which confers a completely different shape to the activation loop. Because of this, the position of Lys211 suffered a large displacement. The behavior of the VRK1(Y213H) mutant differs of the VRK1-WT structure during the MD trajectory. The mutant does not have a close interaction between the specific residues of the activation loop and the residues located in the regulatory C-terminal tail of the

protein, which are required for kinase activation,<sup>30,41</sup> and this structural change predicts a loss of kinase activity.

### The VRK1(Y213H) variant kinase is functionally deficient

To determine the functional effect of the VRK1(Y213H) mutant, we performed in vitro kinase assays using several of the known VRK1 substrates. These included histones H3 and H2AX associated with chromatin remodeling,<sup>13</sup>

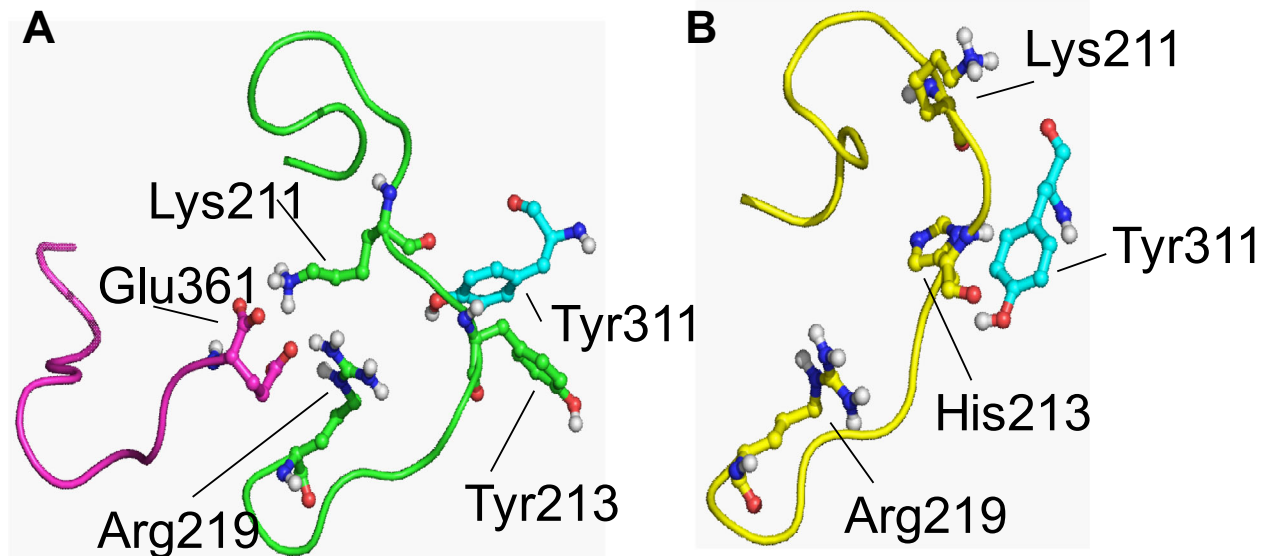


**Figure 2.** Structural modeling of the human VRK1-Y213H variant protein. (A) Structure of the wild-type VRK1 activation loop after 200 nsec of free molecular dynamics. Position of C-terminal tail interacting with the activation loop is indicated (magenta). The activation loop is colored in green. Position of residues Tyr213, Tyr311 (blue, not in the activation loop), Lys211, Arg219 and Glu361 (grey, located in the C-terminal tail) is indicated. (B) Structure of the activation loop of VRK1-Y213H variant after 200 nsec of free molecular dynamics. Note the displacement of the loop compared to the wild-type structure and the different position of the mutated residue (His213). No interaction was detected between the mutated activation loop and the C-terminal tail of VRK1.

coilin required for Cajal body formation,<sup>7</sup> p53,<sup>42</sup> and 53BP1<sup>39</sup> involved in different aspects of DNA damage responses.<sup>43</sup> The mutant VRK1(Y213H) was compared with the wild-type VRK1. In the kinase assays, the effect of the p.Y213H mutant was common to all substrates. There was a significant loss regarding the phosphorylation of histone H3, (Fig. 3A), histone H2AX (Fig. 3B), coilin (Fig. 3C), p53 (Fig. 3D), and 53BP1 (Fig. 3E).

### Protein stability of the VRK1(Y213H) mutant

Several of the known VRK1 mutants associated with neurological phenotypes also have a reduced protein stability.<sup>34</sup> Therefore, we tested the stability of p.Y213H compared to the normal VRK1 protein. Plasmids expressing both proteins were transfected in 293T cells, which were treated with cycloheximide, and the level of protein was determined at different time points. The p.Y213H mutant protein was slightly less stable than normal VRK1 (Fig. S3).

### Effect of the VRK1(Y213H) mutant on the formation of Cajal bodies

Phosphorylation of coilin regulates the assembly and stability of Cajal bodies.<sup>7,44</sup> Therefore, we studied the possible effect of the Y213H mutant on the formation of Cajal

bodies. For this purpose, we used HeLa cells in which the endogenous human VRK1 was depleted by siRNA. These human VRK1 depleted cells were transfected with the murine VRK1, either wild-type (mVRK1) or containing the Y213H mutant (mVRK1-Y213H). In transfected cells depleted of human endogenous VRK1 there was a loss of Cajal bodies, and this effect was rescued in cells expressing the murine wild-type VRK1, but not by the murine VRK1-Y213H mutant protein (Fig. 4).

### Discussion

The heterogeneity of the neuromotor syndromes associated with VRK1 pathogenic variants suggest that their contribution is likely to be mediated by downstream direct targets. All pathogenic variants have in common two possible effects. Some have a reduction of the mutant protein stability, which leads to reduced protein levels. Others have a reduction of their kinase activity with respect to several of its known specific target proteins,<sup>34</sup> some of which are already associated with neurological development and diseases, such as proteins regulating chromatin epigenetic changes, neural development or response to cellular stress and DNA damage.

In this report, we have shown that the VRK1(Y213H) mutant protein is unable to phosphorylate several of its substrates including histone H3, H2AX, p53, 53BP1, and

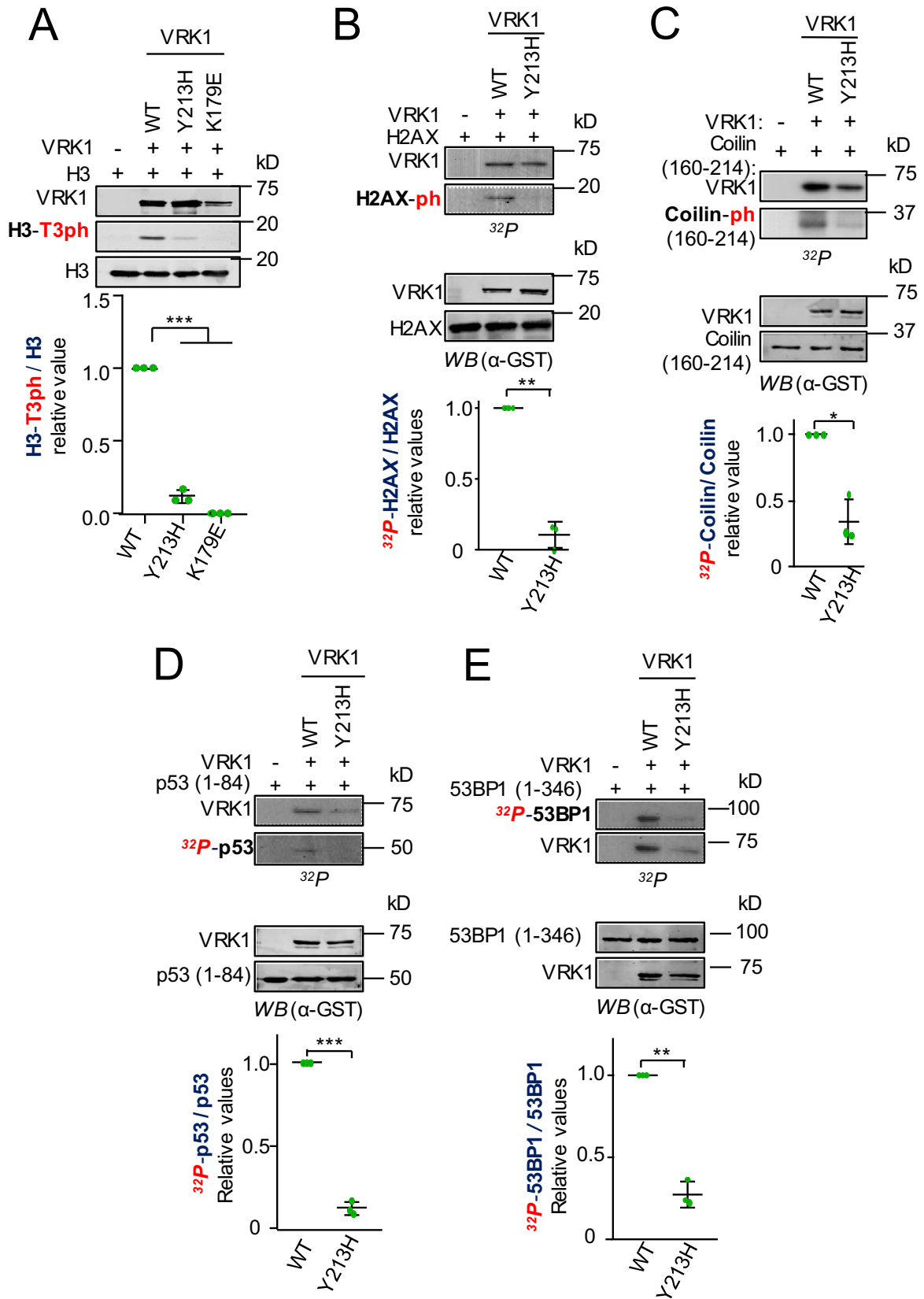


**Figure 3.** Kinase activity of the wild-type VRK1 and mutant VRK1-Y213H using different phosphorylation substrates. (A) Phosphorylation of histone H3 by wild-type VRK1 (WT), VRK1-T213H and kinase-dead VRK1-K179E in Thr3 detected with a phospho-specific antibody. (B) Phosphorylation of histone H2AX in a radioactive kinase assay. (C) Phosphorylation of coilin in a radioactive kinase assay. (D) Phosphorylation of p53 in a radioactive kinase assay. (E) Phosphorylation of 53BP1 in a radioactive kinase assay. One representative gel is shown, and the three independent experiments are shown in Figure S2.

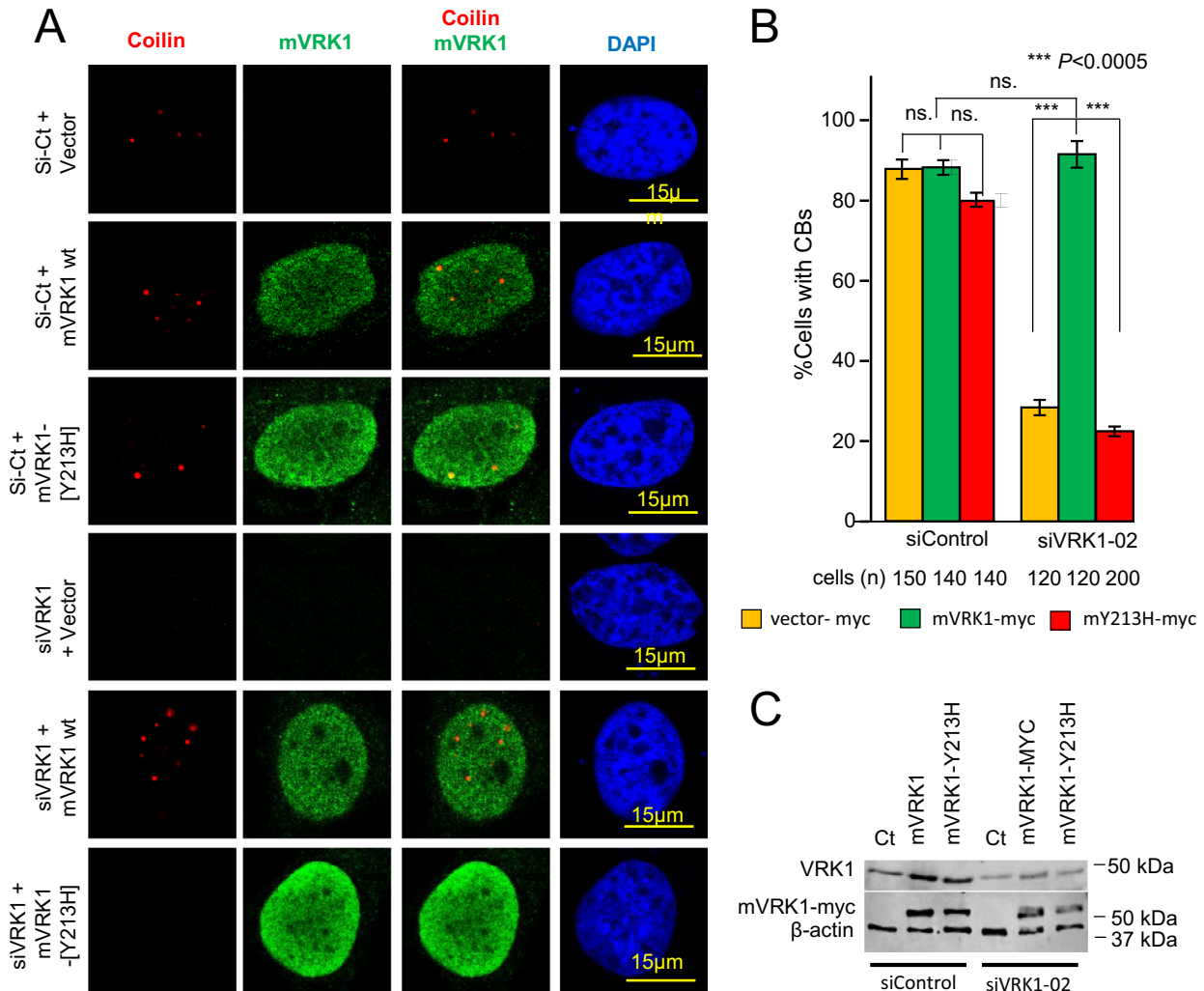


**Figure 4.** Rescue of Cajal body formation by wild-type VRK1 and mutant VRK1-Y213H. Endogenous human VRK1 was depleted with si-VRK1-02 and cells were transfected with either murine VRK1 wild-type (muVRK1) or with the murine VRK1 Y213H variant (muVRK1-Y213H). (A) Images of confocal microscopy showing the presence or absence of Cajal bodies assembled on coilin (red). (B) Quantification of the presence or absence of Cajal bodies in cells that after depletion of endogenous human VRK1 were transfected with either wild-type or the Y213H mutant murine VRK1. (C) Immunoblot to show the depletion of endogenous human VRK1 and its replacement by either murine VRK1 or the murine Y213H VRK1 mutant.

coilin, all of them are pathogenically associated with hereditary neurological/neuromotor syndromes. Functionally, this impaired VRK1 kinase activity implicates a loss of functions, which have to be linked to distal motor neuropathies and SMA phenotype. The most likely intermediate step in

the pathogenesis VRK1(Y213H) is a consequence of the inability of the Y213H mutant protein to phosphorylate and regulate coilin, which can alter its associated proteins and functions. Coilin is the scaffold protein of Cajal Bodies<sup>45</sup> discovered more than one hundred years ago,<sup>46</sup>

which forms a complex with SMN1 in SMA.<sup>6</sup> However, the function of Cajal bodies is not well understood, but it is a ribonucleoprotein complex that participates in RNA processing.<sup>47,48</sup> In a murine coilin knockout models there is a failure to recruit SMN1 to defective or absent CBs.<sup>49,50</sup> All human VRK1 mutant proteins, directly or indirectly fail to form CBs<sup>7,34,51</sup> and mimic the coilin knockout. Furthermore, SMN1 protects against mutant SOD1 toxicity.<sup>52</sup> Mutations in SOD1 disrupt the recruitment of SMN1 to Cajal bodies,<sup>53</sup> and mutations in VCP (valosin) contribute to development of ALS in KO mice,<sup>54</sup> all these proteins form complexes with VRK1 (unpublished).

Most of the known human VRK1 pathogenic variants are unable to form CBs,<sup>34</sup> as it also occurs with the Y213H mutant. Moreover, in cells obtained from patients with compound R219L/W254L mutations, there are no CBs in motor neurons derived from human induced pluripotent stem cells.<sup>51</sup> In a murine model, the human VRK1(R358X) mutant impairs cell cycle progression and migration of neuronal progenitors in early embryogenesis.<sup>55</sup> Moreover, VRK1 partial knockdown in mice causes a motor dysfunction.<sup>56</sup> Nuclear bodies, such as CBs, are regulated during embryogenesis,<sup>57</sup> and their alteration is very likely to cause neurological disorders. In this context, VRK1 regulates the assembly and disassembly of CB mediated by a specific phosphorylation of coilin that controls its stability and the formation of complexes with other proteins.<sup>7</sup> Thus, functionally deficient VRK1 mutations alter the physiological dynamics of CBs, and consequently of its associated proteins and functions. This has been shown to be the case for Y213H (this report) and for other mutants.<sup>34</sup> The heterogeneity of the VRK1 mutations suggests that there might be differences in their specific protein interactions that lead to some heterogeneity among the associated neuromotor syndromes by altering the functionality of Cajal bodies.

Another target of VRK1, p53, regulates WRAP53 that is required for CB formation and maintenance of genome integrity,<sup>58,59</sup> but the activation of p53 by phosphorylation is impaired in the case of the VRK1(Y213H) mutant protein. CBs are associated with ribonucleoproteins complexes involved in RNA processing, but the consequences of their alteration is unknown.<sup>47,60</sup> In the CBs assembled on coilin there are other proteins such as SMN1, associated with SMA,<sup>4</sup> VCP associated with amyotrophic lateral sclerosis (ALS),<sup>61</sup> and ataxin 1 (ATXN1) associated with ataxia.<sup>62</sup> Alterations in any of them cause a distal neuromotor phenotype.

All the VRK1 mutants are either homozygous or compound heterozygous. The heterogeneity of the neurological phenotypes associated with VRK1 pathogenic variants has some common features. All patients presented a functional alteration of motor neuron function, mainly as

distal motor neuropathies, spinal muscular atrophy (SMA) or amyotrophic lateral sclerosis (ELA). However, they differed in their severity and age of presentation, although initial symptoms started during infancy in most cases and are progressive. There are also important differences in intellectual ability ranging from normal to very severe deficiency. Some additional neurological symptoms are associated. This heterogeneity is unlikely to be only the result of the specific VRK1 mutant, since molecularly they have a similar defective function,<sup>34</sup> but rather by the contribution of additional variants in other genes, which differ among patients. However, when more than one case occurs within a family sharing the same mutant, the phenotype is similar among the affected family members.<sup>17</sup>

An alternative pathogenic mechanism implicating the contribution of VRK1 may be a consequence of its interaction with GARS,<sup>41</sup> a gene whose mutations are also associated with distal neuropathies.<sup>63–65</sup> However, the role of aminoacyl-tRNA-synthetases in these diseases is unknown, but may be a consequence of altering neurite formation<sup>66</sup> and peripheral axons.<sup>67,68</sup>

We conclude that VRK1 mutations, associated with distal neuromotor syndromes of unknown origin, should be considered as a rare underlying pathogenic mechanism. Since defective CBs assembly and associated functions are common to a group of heterogeneous distal neuromotor syndromes, whose final neurological phenotype will be determined by the genetic background of the affected individual. Distal motor neuropathies are a consequence of a mutation in any of the different components of nuclear suborganelles, such as CBs, and which lead to this group of related neurological phenotypes.

## Acknowledgments

The computational support of the “Centro de Computación Científica CCC-UAM” is gratefully recognized.

## Conflict of Interest

The authors declare they have no competing conflict of interest.

## Author Contributions

ATM, MS-P, and LA performed the genetic and sequencing study. EM-D and PM-G performed biochemical and cell biology studies, IM-A and PG-P performed molecular structural analysis, JMN-P, and PAL planned the work and coordinated clinical and molecular studies. PAL wrote the final version of the manuscript that was revised and approved by all authors.



## Informed Consent

The parents and the affected patient provided written consent to perform the genetic study.

## Consent to Publish

Written informed consent for publication was obtained from the participants in the study.

## Data Availability Statement

### Database submission

The *VRK1* mutation is available in ClinVar with the variation ID 812546. <https://www.ncbi.nlm.nih.gov/clinvar/variation/812546/>

### Primary source data files availability in open access repositories

WES datasets are available at <https://www.ncbi.nlm.nih.gov/sra/PRJNA606693>.

## References

- Rossor AM, Kalmar B, Greensmith L, Reilly MM. The distal hereditary motor neuropathies. *J Neurol Neurosurg Psychiatry* 2012;83:6–14.
- Rossor AM, Tomaselli PJ, Reilly MM. Recent advances in the genetic neuropathies. *Curr Opin Neurol* 2016;29:537–548.
- Wee CD, Kong L, Sumner CJ. The genetics of spinal muscular atrophies. *Curr Opin Neurol* 2010;23:450–458.
- Singh RN, Howell MD, Ottesen EW, Singh NN. Diverse role of survival motor neuron protein. *Biochim Biophys Acta Gene Regul Mech* 2017;1860:299–315.
- Singh RN, Singh NN. A novel role of U1 snRNP: splice site selection from a distance. *Biochim Biophys Acta Gene Regul Mech* 2019;1862:634–642.
- Hebert MD, Szymczyk PW, Shpargel KB, Matera AG. Coilin forms the bridge between Cajal bodies and SMN, the spinal muscular atrophy protein. *Genes Dev* 2001;15:2720–2729.
- Cantarero L, Sanz-Garcia M, Vinograd-Byk H, et al. VRK1 regulates Cajal body dynamics and protects coilin from proteasomal degradation in cell cycle. *Sci Rep* 2015;5:10543.
- Girard C, Neel H, Bertrand E, Bordonne R. Depletion of SMN by RNA interference in HeLa cells induces defects in Cajal body formation. *Nucleic Acids Res* 2006;34:2925–2932.
- Enwerem II, Wu G, Yu YT, Hebert MD. Cajal body proteins differentially affect the processing of box C/D scaRNPs. *PLoS One* 2015;10:e0122348.
- Jady BE, Darzacq X, Tucker KE, et al. Modification of Sm small nuclear RNAs occurs in the nucleoplasmic Cajal body following import from the cytoplasm. *EMBO J* 2003;22:1878–1888.
- Lemm I, Girard C, Kuhn AN, et al. Ongoing U snRNP biogenesis is required for the integrity of Cajal bodies. *Mol Biol Cell* 2006;17:3221–3231.
- Sabra M, Texier P, El Maalouf J, Lomonte P. The Tudor protein survival motor neuron (SMN) is a chromatin-binding protein that interacts with methylated lysine 79 of histone H3. *J Cell Sci* 2013;126(Pt 16):3664–3677.
- Salzano M, Sanz-Garcia M, Monsalve DM, et al. VRK1 chromatin kinase phosphorylates H2AX and is required for foci formation induced by DNA damage. *Epigenetics* 2015;10:373–383.
- Whittom AA, Xu H, Hebert MD. Coilin levels and modifications influence artificial reporter splicing. *Cell Mol Life Sci* 2008;65:1256–1271.
- Choi YH, Lim JK, Jeong MW, Kim KT. HnRNP A1 phosphorylated by VRK1 stimulates telomerase and its binding to telomeric DNA sequence. *Nucleic Acids Res* 2012;40:8499–8518.
- Previtali SC, Zhao E, Lazarevic D, et al. Expanding the spectrum of genes responsible for hereditary motor neuropathies. *J Neurol Neurosurg Psychiatry* 2019;90:1171–1179.
- Renbaum P, Kellerman E, Jaron R, et al. Spinal muscular atrophy with pontocerebellar hypoplasia is caused by a mutation in the VRK1 gene. *Am J Hum Genet* 2009;85:281–289.
- Gonzaga-Jauregui C, Lotze T, Jamal L, et al. Mutations in VRK1 associated with complex motor and sensory axonal neuropathy plus microcephaly. *JAMA Neurol* 2013;70:1491–1498.
- Nguyen TP, Biliciler S, Wiszniewski W, Sheikh K. Expanding phenotype of VRK1 mutations in motor neuron disease. *J Clin Neuromuscul Dis* 2015;17:69–71.
- Stoll M, Teoh H, Lee J, et al. Novel motor phenotypes in patients with VRK1 mutations without pontocerebellar hypoplasia. *Neurology* 2016;87:65–70.
- Feng SY, Li LY, Feng SM, Zou ZY. A novel VRK1 mutation associated with recessive distal hereditary motor neuropathy. *Ann Clin Transl Neurol* 2019;6:401–405.
- Greenbaum L, Barel O, Nikitin V, et al. Identification of a homozygous VRK1 mutation in two patients with adult-onset distal hereditary motor neuropathy. *Muscle Nerve* 2019;61(3):395–400.
- Li N, Wang L, Sun X, et al. A novel mutation in VRK1 associated with distal spinal muscular atrophy. *J Hum Genet* 2019;64:215–219.

24. Yamaura G, Higashiyama Y, Kusama K, et al. Novel VRK1 mutations in a patient with childhood-onset motor neuron disease. *Intern Med* 2019;58:2715–2719.
25. Sung A, Moretti P, Shaibani A. Two cases of spinal muscular atrophy due to mutations in the VRK1 gene (P4.4-005). *Neurology* 2019;92(15 Supplement):P4.-005.
26. Richards S, Aziz N, Bale S, et al. Standards and guidelines for the interpretation of sequence variants: a joint consensus recommendation of the American College of Medical Genetics and Genomics and the Association for Molecular Pathology. *Genet Med* 2015;17:405–424.
27. Aziz N, Zhao Q, Bry L, et al. College of American Pathologists' laboratory standards for next-generation sequencing clinical tests. *Arch Pathol Lab Med* 2015;139:481–493.
28. Adzhubei IA, Schmidt S, Peshkin L, et al. A method and server for predicting damaging missense mutations. *Nat Methods* 2010;7:248–249.
29. Stelzer G, Plaschkes I, Oz-Levi D, et al. VarElect: the phenotype-based variation prioritizer of the GeneCards Suite. *BMC Genom* 2016;17(Suppl 2):444.
30. Shin J, Chakraborty G, Bharatham N, et al. NMR solution structure of human vaccinia-related kinase 1 (VRK1) reveals the C-terminal tail essential for its structural stability and autocatalytic activity. *J Biol Chem* 2011;286:22131–22138.
31. Vazquez-Cedeira M, Barcia-Sanjurjo I, Sanz-Garcia M, et al. Differential inhibitor sensitivity between human kinases VRK1 and VRK2. *PLoS One* 2011;6:e23235.
32. Lopez-Borges S, Lazo PA. The human vaccinia-related kinase 1 (VRK1) phosphorylates threonine-18 within the mdm-2 binding site of the p53 tumour suppressor protein. *Oncogene* 2000;19:3656–3664.
33. Moura DS, Campillo-Marcos I, Vazquez-Cedeira M, Lazo PA. VRK1 and AURKB form a complex that cross inhibit their kinase activity and the phosphorylation of histone H3 in the progression of mitosis. *Cell Mol Life Sci* 2018;76:2591–2611.
34. Martin-Doncel E, Rojas AM, Cantarero L, Lazo PA. VRK1 functional insufficiency due to alterations in protein stability or kinase activity of human VRK1 pathogenic variants implicated in neuromotor syndromes. *Sci Rep* 2019;9:13381.
35. Barcia-Sanjurjo I, Vazquez-Cedeira M, Barcia R, Lazo PA. Sensitivity of the kinase activity of human vaccinia-related kinase proteins to toxic metals. *J Biol Inorg Chem* 2013;18:473–482.
36. Moura DS, Fernandez IF, Marin-Royo G, et al. Oncogenic Sox2 regulates and cooperates with VRK1 in cell cycle progression and differentiation. *Sci Rep* 2016;6:28532.
37. Lopez-Sanchez I, Valbuena A, Vazquez-Cedeira M, et al. VRK1 interacts with p53 forming a basal complex that is activated by UV-induced DNA damage. *FEBS Lett* 2014;588:692–700.
38. Santos CR, Vega FM, Blanco S, et al. The vaccinia virus B1R kinase induces p53 downregulation by an Mdm2-dependent mechanism. *Virology* 2004;328:254–265.
39. Sanz-Garcia M, Monsalve DM, Sevilla A, Lazo PA. Vaccinia-related Kinase 1 (VRK1) is an upstream nucleosomal kinase required for the assembly of 53BP1 foci in response to ionizing radiation-induced DNA damage. *J Biol Chem* 2012;287:23757–23768.
40. Chelli R, Gervasio FL, Procacci P, Schettino V. Stacking and T-shape competition in aromatic-aromatic amino acid interactions. *J Am Chem Soc* 2002;124:6133–6143.
41. Sanz-Garcia M, Vazquez-Cedeira M, Kellerman E, et al. Substrate profiling of human vaccinia-related kinases identifies coilin, a Cajal body nuclear protein, as a phosphorylation target with neurological implications. *J Proteomics* 2011;75:548–560.
42. Campillo-Marcos I, Lazo PA. Olaparib and ionizing radiation trigger a cooperative DNA-damage repair response that is impaired by depletion of the VRK1 chromatin kinase. *J Exp Clin Cancer Res* 2019;38:203.
43. Campillo-Marcos I, Lazo PA. Implication of the VRK1 chromatin kinase in the signaling responses to DNA damage: a therapeutic target? *Cell Mol Life Sci* 2018;75:2375–2388.
44. Hebert MD, Poole AR. Towards an understanding of regulating Cajal body activity by protein modification. *RNA Biol* 2017;14:761–778.
45. Cioce M, Lamond AI. Cajal bodies: a long history of discovery. *Annu Rev Cell Dev Biol* 2005;21:105–131.
46. Ramon y Cajal S. Un sencillo metodo de coloracion selectiva del reticulo protoplasmatico y sus efectos en los diversos organos nerviosos de vertebrados e invertebrados. *Trab Lab Invest Biol* 1903;2:129–221.
47. Boulisfane N, Choleza M, Rage F, et al. Impaired minor tri-snRNP assembly generates differential splicing defects of U12-type introns in lymphoblasts derived from a type I SMA patient. *Hum Mol Genet* 2011;20:641–648.
48. Nizami Z, Deryusheva S, Gall JG. The Cajal body and histone locus body. *Cold Spring Harbor Perspect Biol* 2010;2:a000653.
49. Tucker KE, Berciano MT, Jacobs EY, et al. Residual Cajal bodies in coilin knockout mice fail to recruit Sm snRNPs and SMN, the spinal muscular atrophy gene product. *J Cell Biol* 2001;154:293–307.
50. Morse R, Shaw DJ, Todd AG, Young PJ. Targeting of SMN to Cajal bodies is mediated by self-association. *Hum Mol Genet* 2007;16:2349–2358.
51. El-Bazzal L, Rihan K, Bernard-Marissal N, et al. Loss of Cajal bodies in motor neurons from patients with novel mutations in VRK1. *Hum Mol Genet* 2019;28:2378–2394.
52. Zou T, Ilangovan R, Yu F, et al. SMN protects cells against mutant SOD1 toxicity by increasing chaperone

- activity. *Biochem Biophys Res Commun* 2007;364:850–855.
53. Kariya S, Re DB, Jacquier A, et al. Mutant superoxide dismutase 1 (SOD1), a cause of amyotrophic lateral sclerosis, disrupts the recruitment of SMN, the spinal muscular atrophy protein to nuclear Cajal bodies. *Hum Mol Genet* 2012;21:3421–3434.
  54. Yin HZ, Nalbandian A, Hsu CI, et al. Slow development of ALS-like spinal cord pathology in mutant valosin-containing protein gene knock-in mice. *Cell Death Dis* 2012;3:e374.
  55. Vinograd-Byk H, Sapir T, Cantarero L, et al. The spinal muscular atrophy with pontocerebellar hypoplasia gene VRK1 regulates neuronal migration through an amyloid-beta precursor protein-dependent mechanism. *J Neurosci* 2015;35:936–942.
  56. Vinograd-Byk H, Renbaum P, Levy-Lahad E. Vrk1 partial knockdown in mice results in reduced brain weight and mild motor dysfunction, and indicates neuronal VRK1 target pathways. *Sci Rep* 2018;8:11265.
  57. Arias Escayola D, Neugebauer KM. Dynamics and function of nuclear bodies during embryogenesis. *Biochemistry* 2018;57:2462–2469.
  58. Mahmoudi S, Henriksson S, Weibrecht I, et al. WRAP53 is essential for Cajal body formation and for targeting the survival of motor neuron complex to Cajal bodies. *PLoS Biol* 2010;8:e1000521.
  59. Henriksson S, Farnebo M. On the road with WRAP53beta: guardian of Cajal bodies and genome integrity. *Front Genet* 2015;6:91.
  60. Poole AR, Hebert MD. SMN and coilin negatively regulate dyskerin association with telomerase RNA. *Biol Open* 2016;5:726–735.
  61. Abramzon Y, Johnson JO, Scholz SW, et al. Valosin-containing protein (VCP) mutations in sporadic amyotrophic lateral sclerosis. *Neurobiol Aging* 2012;33:2231.e1–2231.e6.
  62. Hong S, Ka S, Kim S, et al. p80 coilin, a coiled body-specific protein, interacts with ataxin-1, the SCA1 gene product. *Biochim Biophys Acta* 2003;1638:35–42.
  63. Dubourg O, Azzedine H, Yaou RB, et al. The G526R glycyI-tRNA synthetase gene mutation in distal hereditary motor neuropathy type V. *Neurology* 2006;66:1721–1726.
  64. Seburn KL, Nangle LA, Cox GA, et al. An active dominant mutation of glycyI-tRNA synthetase causes neuropathy in a Charcot-Marie-Tooth 2D mouse model. *Neuron* 2006;51:715–726.
  65. Motley WW, Talbot K, Fischbeck KH. GARS axonopathy: not every neuron's cup of tRNA. *Trends Neurosci* 2010;33:59–66.
  66. Nangle LA, Zhang W, Xie W, et al. Charcot-Marie-Tooth disease-associated mutant tRNA synthetases linked to altered dimer interface and neurite distribution defect. *Proc Natl Acad Sci USA* 2007;104:11239–11244.
  67. Antonellis A, Lee-Lin SQ, Wasterlain A, et al. Functional analyses of glycyI-tRNA synthetase mutations suggest a key role for tRNA-charging enzymes in peripheral axons. *J Neurosci* 2006;26:10397–10406.
  68. Banks GT, Bros-Facer V, Williams HP, et al. Mutant glycyI-tRNA synthetase (Gars) ameliorates SOD1(G93A) motor neuron degeneration phenotype but has little effect on Loa dynein heavy chain mutant mice. *PLoS One* 2009;4:e6218.

## Supporting Information

Additional supporting information may be found online in the Supporting Information section at the end of the article.

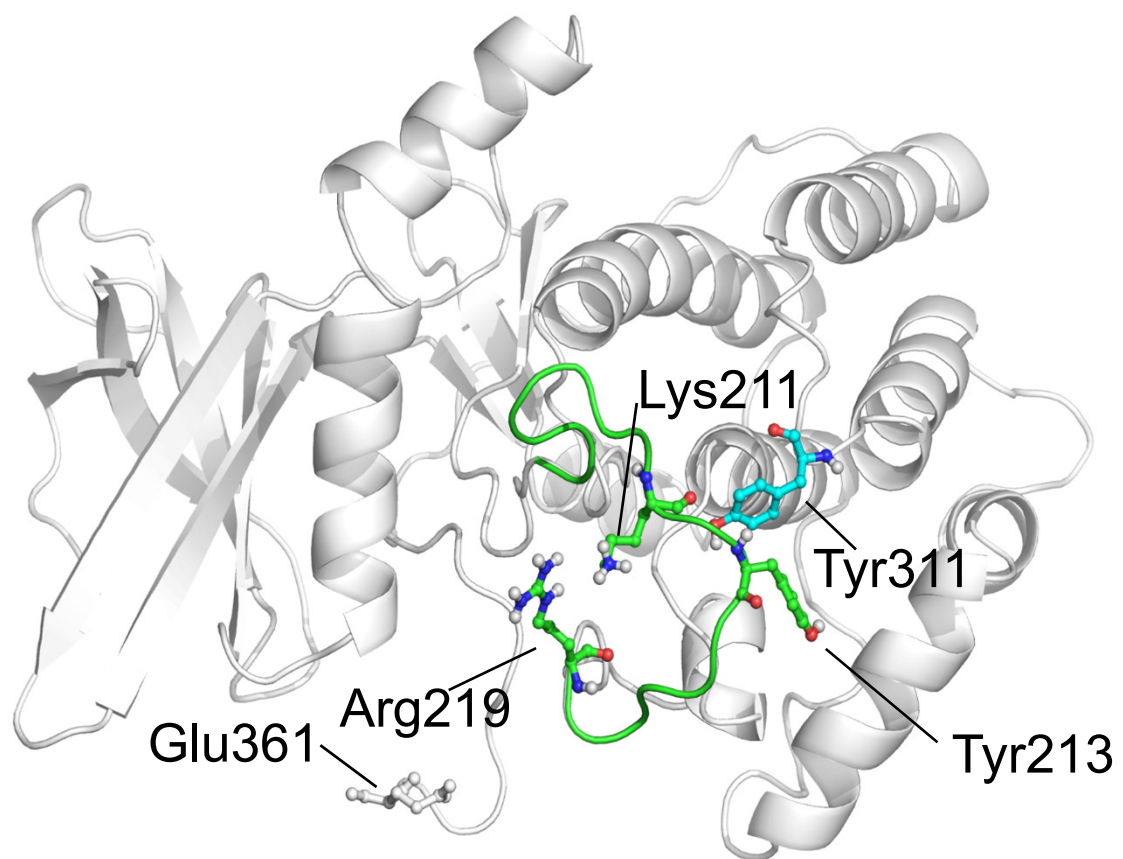
**Figure S1.** Structural modeling of VRK1 Y213H variant. (A) 3D structure of wild-type VRK1 protein (PDB id: 2LAV). The activation loop is colored in green. Position of residues Tyr213, Tyr311 (blue, not in the activation loop), Lys211, Arg219 and Glu361 (grey, located in the C-terminal tail) are indicated.

**Figure S2.** Phosphorylation of several substrates by VRK1 and VRK1-Y213H in triplicate. (A) Histone H3. (B) Histone H2AX. (C) Coilin. (D) TP53. (E) 53BP1.

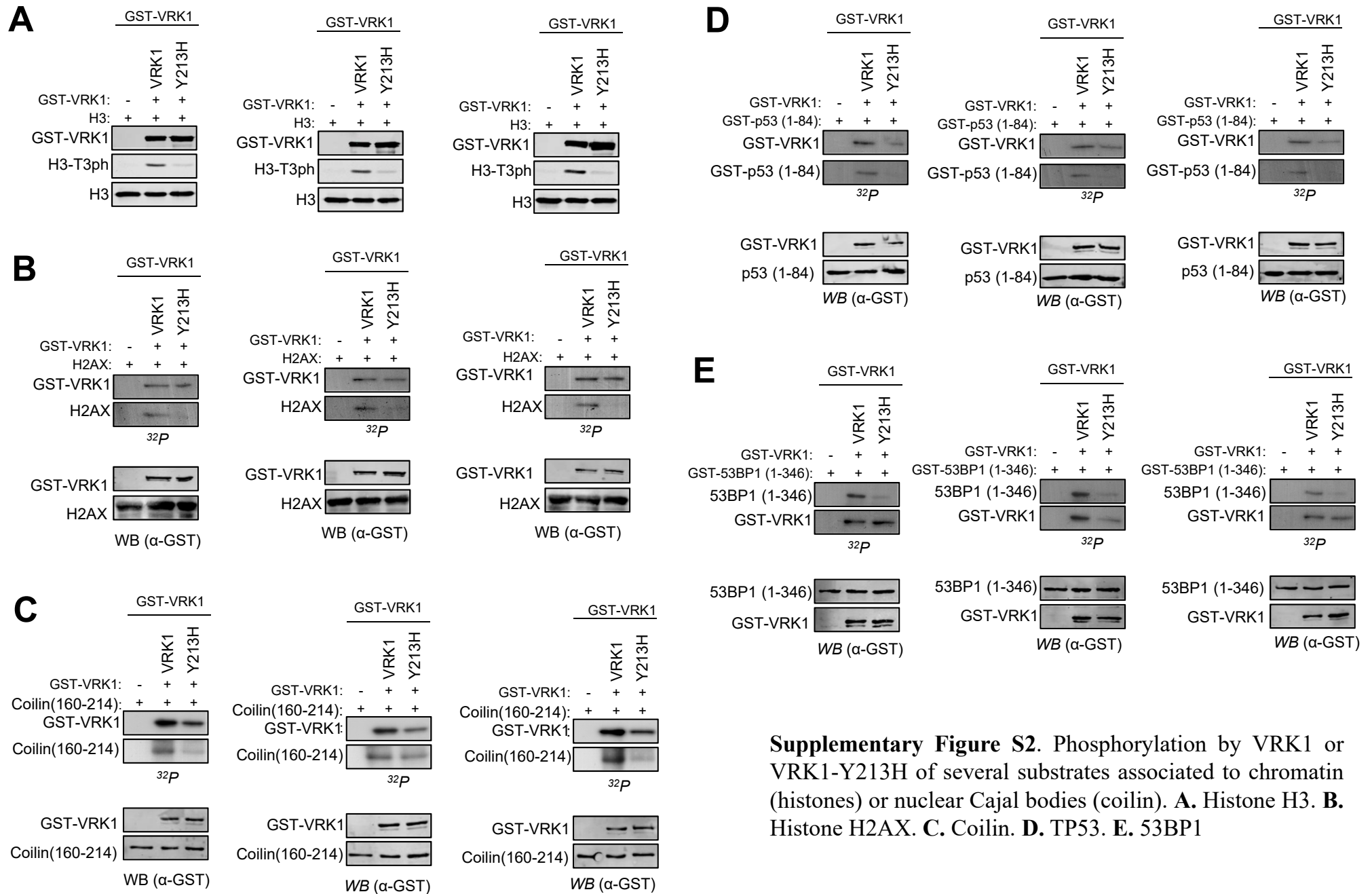
**Figure S3.** Protein stability of the wild-type VRK1 and mutant VRK1-Y213H proteins.

**Table S1.** List of primary and secondary antibodies used in this work.

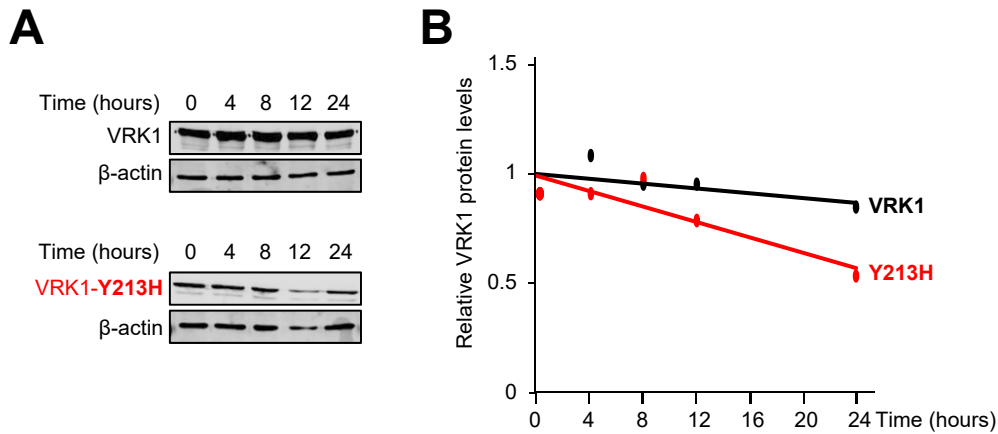
**Data S1.** This refers to databases correctly placed before in the text.



**Supplementary Figure S1.** Structural modeling of VRK1 Y213H variant. (A) 3D structure of wild-type VRK1 protein (PDB id: 2LAV). The activation loop is colored in green. Position of residues Tyr213, Tyr311 (blue, not in the activation loop), Lys211, Arg219 and Glu361 (grey, located in the C-terminal tail) is indicated.



**Supplementary Figure S2.** Phosphorylation by VRK1 or VRK1-Y213H of several substrates associated to chromatin (histones) or nuclear Cajal bodies (coilin). **A.** Histone H3. **B.** Histone H2AX. **C.** Coilin. **D.** TP53. **E.** 53BP1



**Supplementary Figure S3.** Protein stability of the wild-type VRK1 and mutant VRK1-Y213H proteins. Plasmids expressing human VRK1 or VRK1-Y213H tagged with the HA-epitope were cloned in plasmid pCEFL-HA vector and transfected in HEK293T cells. Cycloheximide was added to the culture to block gene transcription. The level of VRK1 proteins after cycloheximide addition were determined in western blots. **A.** The experiment was performed in triplicate and a representative gel is shown. **B.** The relative level of each protein at different times was quantitated and shown in the graph (B).

**Supplementary Table S1.** List of primary and secondary antibodies used in this work.

<b>Antibody</b>	<b>Type</b>	<b>Dilution WB</b>	<b>Clone and/or reference</b>	<b>Supplier</b>
GST-Tag	Mouse monoclonal	1:1000	B14/sc-138	Santa Cruz
HA-Tag	Mouse monoclonal	1:1000	F7/sc-7392	Santa Cruz
Histone H3	Rabbit polyclonal	1:1000	9175	Cell Signaling
Phospho-histone H3 (Thr3ph)	Rabbit polyclonal	1:1000	05-746R	Merck-Millipore
coilin	Mouse monoclonal	1:200	sc-56298	Santa Cruz
$\beta$ -actin	Mouse monoclonal	1:1000	AC15/A5441	Sigma-Aldrich
Goat Anti-Mouse IgG, DyLight 680	Goat	1:10000	35518	Thermo Scientific
Goat Anti-Rabbit IgG, DyLight 800	Goat	1:10000	35571	Thermo Scientific
Anti-Mouse IgG-HRP	Sheep	1:10000	NA931V	Amersham Biosciences;

## Supplementary material and methods

### Structural modeling of VRK1-Y213H variant

The 3D structure of the human Vaccinia-Related Kinase 1 (VRK1) wild-type protein was obtained from the Protein Data Bank (PDB id: 2LAV)[1]. The first conformer (of the 20 NMR conformers included in the PDB file) was selected for further processing. Model for VRK1-Y213H variant was generated using the wild-type structure as template. Models were built using the SWISS-MODEL server (<http://swissmodel.expasy.org>) and their structural quality were within the range of those accepted for homology-based structure (Anolea/Gromos/QMEAN4) [2].

### Molecular Dynamics simulation

Prior to molecular dynamics (MD) procedures, 3D structures were energy minimized using the GROMOS 43B1 force field implemented in DeepView (<http://spdbv.vital-it.ch/>), using 500 steps of steepest descent minimization followed by 500 steps of conjugate-gradient minimization.

Wild-type VRK1 structure and VRK1-Y213H model were subjected to 200 ns of MD simulation using the AMBER18 molecular dynamics package (<http://ambermd.org/>; University of California-San Francisco, CA). The 3D structures were solvated with a periodic octahedral pre-equilibrated solvent box using the LEaP module of AMBER, with 12 Å as the shortest distance between any atom in the protein subdomain and the periodic box boundaries. Free MD simulation were performed essentially as previously described [3], using the PMEMD program of AMBER18 and the ff14SB force field (<http://ambermd.org/>). The SHAKE algorithm was used, allowing a time step of 2 fs. Systems were initially relaxed over 15,000 steps of energy minimization with a cut-off of 12 Å. Simulations were then started with a 20 ps heating phase, raising the temperature from 0 to 300 K in 10 temperature change steps, after each of which velocities were reassigned. During minimization and heating, the C $\alpha$  trace dihedrals were restrained with a force constant of 500 kcal mol<sup>-1</sup> rad<sup>-2</sup> and gradually released in an equilibration phase in which the force constant was progressively reduced to 0 over 200 ps. After the equilibration phase, 200 ns of unrestricted MD simulation were obtained. MD trajectories were analyzed using VMD software [4]. The trajectories were continuously monitored by the measurement of root-mean square deviation (RMSD).



Figures were generated using the Pymol Molecular Graphics System (<https://pymol.org/>; Schrödinger, LLC, Portland, OR).

### **Plasmids and mutagenesis**

Human VRK1 was expressed from mammalian expression vector, pCEFL-HA-VRK1 [5], and bacterial expression pGEX-4T-VRK1 [5-8]. The following primers were used to generate the Y213H mutations in human and murine VRK1. Mutations in VRK1 were performed using the GeneArt Site-Directed Mutagenesis System (Invitrogen-ThermoFisher) with the following primers for human VRK1-Y213H forward (5'-AGGAGTTCATAAAGAACACAAAGAAGACCCCAAAA-3') and reverse (5'-TTTTGGGGTCTTCTTTGTGTTCTTTATGAACTCCT-3'); and for murine VRK1-Y213H forward (5'-TGGAGTTCATAAAGAGCACAAAGGAAGATCCCAAAA-3') and reverse (5'-TTTGGGATCTTCCTTGTACTCTTTATGAACTCCA-3'). Sanger sequencing was used to confirm all variants generated.

Human VRK1 wild type and the VRK1-Y213H variant were expressed from constructs pGEX4T-GST-VRK1 plasmid expressed in *E.coli* BL21 strain competent cells. The following plasmids were used to express the substrates: pGST4T-53BP1 (1-346) [9, 10]; GST-p53(1-85)[11] [6, 12], and pGEX4T-GST-Coilin(160-214) [13]. All plasmids were expressed in BL21 *E.coli* to purify the fusion protein used as substrate in kinase assays as previously reported [8, 13]. Human H3 is a purified recombinant protein (Merck-Millipore).

### **Kinase assays**

The kinase assays were performed as previously described [5, 8, 14]. Briefly, In vitro kinase assays with [<sup>32</sup>-P]- $\gamma$ ATP were performed with GST-VRK1 wild-type and variants [5, 13, 15]. Assays with the following substrates were previously published: p53 [12, 16], histone H3 [7, 17], 53BP1 [10], and GST-coilin [13].

The Serine-Threonine kinase activity of VRK1 was analysed by performing in vitro kinase assays using 2  $\mu$ g of GST-VRK1 and variant recombinant proteins that were purified from BL21 cells. The following proteins (2  $\mu$ g) were used as specific substrates, GST-53bp1(1-346) [10], GST-Coilin(160-214) [13], GST-p53(1-84) [6, 18, 19], and human recombinant histones H3 [7, 17]. To perform the in vitro kinase assay [19], it was used a specific buffer (20mM Tris-HCl pH 7.5, 5mM MgCl<sub>2</sub>, 0.5mM DTT

and 150mM KCl), 5 $\mu$ M ATP and 5 $\mu$ Ci (0.1 $\mu$ M) radiolabelled [ $\gamma$ -<sup>32</sup>P]ATP in a final volume of 40 $\mu$ l during 45 min at 30°C [8]. H3T3ph was detected with a rabbit polyclonal antibody (Upstate-Millipore) [15, 17]. In radioactive assays, film exposure was in the lineal response range for all assays.

### **Electrophoresis, antibodies and immunoblots**

Proteins were separated in SDS-PAGE gels in running buffer (25mM Tris-HCl, pH 8.0, 200mM glycine, 1.7mM SDS), and transferred to a PVDF membrane (Immobilon-FL, Millipore) in buffer (25mM Tris-HCl, pH 8.0, 19.2 mM glycine, 15% methanol) as previously described [13, 15, 20, 21]. The primary and secondary antibodies are listed in Supplementary Table S1. The secondary antibodies were incubated for an hour and the fluorescence was detected with LI-COR Odyssey Infrared Imaging System or with ECL Western Blotting Detection Reagent (Sigma-Aldrich) were used if the secondary antibodies were conjugated with peroxidase.

### **Cell lines, transfection and cell lysate**

For the study of Cajal bodies formation, the validated HeLa (ATCC-CCL2) cell line was grown in Dulbecco's Modified Eagle's Medium (DMEM) (Sigma-Aldrich) and transfected using Lipofectin [13, 15, 20]. Cell extracts were prepared by using a mild lysis buffer (50mM Tris-HCl, pH 8.0, 150mM NaCl, 1% Triton X-100 and 1mM EDTA) supplemented with protease inhibitors (1mM PMSF, 10  $\mu$ g/mL aprotinin and 10  $\mu$ g/mL leupeptin) and phosphatase inhibitors (1mM sodium orthovanadate, 1mM NaF) and incubated for 20 minutes [8, 13, 15].

### **Statistical analysis**

Statistical analysis were performed using the IBM SPSS 28 statistics package. All assays were performed in the lineal response range and in identical conditions for all substrates [8]. Individual quantitative experiments were repeated three times, and statistical significance was analyzed using two-tailed T-test with Welch' correction [22].

### **Reagents**

Recombinant human histones H3 and H2AX (Millipore, Merck), Cycloheximide (Sigma-Aldrich). All other chemical were from Sigma-Merck (Darmstadt, Germany).

Tissue culture media and reagents were from GIBCO-ThermoFisher Scientific (Waltham, MA).

## REFERENCES

1. Shin, J., Chakraborty, G., Bharatham, N., Kang, C., Tochio, N., Koshiya, S., Kigawa, T., Kim, W., Kim, K. T. & Yoon, H. S. (2011), *J Biol Chem.* **286**, 22131-8.
2. Benkert, P., Biasini, M. & Schwede, T. (2011), *Bioinformatics.* **27**, 343-50.
3. Marcos-Alcalde, I., Mendieta-Moreno, J. I., Puisac, B., Gil-Rodriguez, M. C., Hernandez-Marcos, M., Soler-Polo, D., Ramos, F. J., Ortega, J., Pie, J., Mendieta, J. & Gomez-Puertas, P. (2017), *Sci Rep.* **7**, 3266.
4. Humphrey, W., Dalke, A. & Schulten, K. (1996), *J Mol Graph.* **14**, 33-8, 27-8.
5. Vazquez-Cedeira, M., Barcia-Sanjurjo, I., Sanz-Garcia, M., Barcia, R. & Lazo, P. A. (2011), *PLoS ONE.* **6**, e23235.
6. Lopez-Borges, S. & Lazo, P. A. (2000), *Oncogene.* **19**, 3656-64.
7. Moura, D. S., Campillo-Marcos, I., Vazquez-Cedeira, M. & Lazo, P. A. (2018), *Cell Mol Life Sci.* **76**, 2591-2611.
8. Martin-Doncel, E., Rojas, A. M., Cantarero, L. & Lazo, P. A. (2019), *Sci Rep.* **9**, 13381.
9. Rappold, I., Iwabuchi, K., Date, T. & Chen, J. (2001), *J Cell Biol.* **153**, 613-20.
10. Sanz-Garcia, M., Monsalve, D. M., Sevilla, A. & Lazo, P. A. (2012), *J Biol Chem.* **287**, 23757-23768.
11. Milne, D. M., Campbell, D. G., Caudwell, F. B. & Meek, D. W. (1994), *J Biol Chem.* **269**, 9253-9260.
12. Lopez-Sanchez, I., Valbuena, A., Vazquez-Cedeira, M., Khadake, J., Sanz-Garcia, M., Carrillo-Jimenez, A. & Lazo, P. A. (2014), *FEBS Lett.* **588**, 692-700.
13. Cantarero, L., Sanz-Garcia, M., Vinograd-Byk, H., Renbaum, P., Levy-Lahad, E. & Lazo, P. A. (2015), *Sci Rep.* **5**, 10543.
14. Barcia-Sanjurjo, I., Vazquez-Cedeira, M., Barcia, R. & Lazo, P. A. (2013), *J Biol Inorg Chem.* **18**, 473-82.
15. Moura, D. S., Fernandez, I. F., Marin-Royo, G., Lopez-Sanchez, I., Martin-Doncel, E., Vega, F. M. & Lazo, P. A. (2016), *Sci Rep.* **6**, 28532.
16. Santos, C. R., Vega, F. M., Blanco, S., Barcia, R. & Lazo, P. A. (2004), *Virology.* **328**, 254-65.
17. Salzano, M., Sanz-Garcia, M., Monsalve, D. M., Moura, D. S. & Lazo, P. A. (2015), *Epigenetics.* **10**, 373-83.
18. Milne, D. M., Palmer, R. H., Campbell, D. G. & Meek, D. W. (1992), *Oncogene.* **7**, 1361-1369.
19. Barcia, R., Lopez-Borges, S., Vega, F. M. & Lazo, P. A. (2002), *Arch Biochem Biophys.* **399**, 1-5.
20. Monsalve, D. M., Campillo-Marcos, I., Salzano, M., Sanz-Garcia, M., Cantarero, L. & Lazo, P. A. (2016), *Biochim Biophys Acta Molecular Cell Research.* **1863**, 760-9.
21. Salzano, M., Vazquez-Cedeira, M., Sanz-Garcia, M., Valbuena, A., Blanco, S., Fernandez, I. F. & Lazo, P. A. (2014), *Oncotarget.* **5**, 1770-1778.
22. Bremer, M. & Doerge, R. M. (2009) *Statistics at the bench: a step-by step handbook for biologists*, Cold Spring Harbor Laboratory Press, New York.